NASA Technical Paper 2668

1987

Electron Stimulated Desorption of Atomic Oxygen From Silver

R. A. Outlaw and
W. K. Peregoy
Langley Research Center
Hampton, Virginia

Gar B. Hoflund and
Gregory R. Corallo
University of Florida
Gainesville, Florida

National Aeronautics
and Space Administration

Scientific and Technical Information Branch

Abstract

The electron stimulated desorption (ESD) of neutral oxygen atoms from polycrystalline silver and of oxygen ions from Ag(110) has been studied. Polycrystalline Ag charged with $^{16}O_2$ and $^{18}O_2$ and bombarded by low-energy electrons ($\approx$100 eV) under ultrahigh vacuum (UHV) conditions emitted O atom flux levels of 1×10^{12} cm^{-2}-s^{-1} at a Ag temperature of 300°C. The flux was detected with a quadrupole mass spectrometer operating in the appearance potential mode. The neutral cross section at about 100°C was determined to be 7×10^{-19} cm^2. Ancillary experiments conducted in a UHV chamber equipped with a cylindrical mirror analyzer and rigged for ion energy distribution and ion angular distribution were used to study O ions desorbed from Ag(110). Two primary O^+ energies of 2.4 and 5.4 eV were detected from the Ag(110) after having been dosed with 2500 L of $^{16}O_2$. It also appears that in both experiments there was strong evidence for directionality of the emitted flux. The results of this study serve as a proof of concept for the development of a laboratory atomic oxygen beam generator that simulates the gas flux environment experienced by orbiting vehicles.

Introduction

The composition of the atmosphere at the orbital altitude (200 to 1000 km) of a spacecraft combined with its orbital velocity ($\approx$8 km-s^{-1}) results in a flux of hyperthermal atomic oxygen (E $\approx$ 5 eV and $\phi \approx 1 \times 10^{15}$ cm^{-2}-s^{-1}) impinging on the spacecraft surfaces. The high chemical reactivity of this atomic oxygen flux has caused substantial degradation of organic materials onboard the Space Shuttle and suggests that materials on the proposed Space Station, composites used in large space structures, exterior coatings on the optics of the Hubble Space Telescope, materials for proposed ultraviolet telescopes, and materials for future laser communications systems may have substantially reduced lifetimes. Therefore, the study of the reaction of these materials with atomic oxygen in ground-based laboratories (ref. 1) is essential. In order to conduct such laboratory experiments, an atomic oxygen beam generator is required that can closely simulate the flux and energy (within the appropriate vacuum environment) which space vehicles experience in orbit.

In addition to its usefulness for studying atomic oxygen reactions with spacecraft materials, such a beam system would also be of importance to NASA in the calibration of mass spectrometers and other detection systems that would be used for mapping the density of the gas constituents within the orbital envelope. The extreme reactivity of atomic oxygen leads to numerous chemical unions with other species to form CO, CO_2, H_2O, O_2, SO_2, and NO_2. Since these unions occur with only a few surface collisions, the atomic oxygen quickly loses its identity. Calibration, therefore, is essential to make accurate measurements of the representative gas environment within the orbital envelope.

A third use for an atomic oxygen beam generator would be in the area of collision dynamics and cross-beam chemical kinetics. The unavailability of a pure, well-behaved oxygen beam (especially in the range of 1 to 10 eV) has limited the determination of atomic oxygen-molecule collision and chemical kinetic cross sections, which are of fundamental interest to physicists and chemists. Other areas of potential use include determination of drag coefficient and basic gas-surface interactions.

Current techniques for forming atomic oxygen beams primarily fall into three categories: radio frequency (rf) discharge, thermal dissociation, and electronic impact (ref. 2). In order to attain a range of energies, several methods of acceleration, such as charge transfer and nozzle expansion, are used. Beams formed through the use of these techniques have some combination of the following problems: low flux intensity, low mean energy, wide energy distribution, numerous excited states of oxygen and accompanying gases, and synergistic reactions from different species. Furthermore, contaminating background densities within the experimental system often mask the true interaction between atomic oxygen and the material sample. For example, if the background pressure is 1×10^{-6} torr, the entire surface of a sample is covered in 1 s by gases other than atomic oxygen (such as CO or O_2), with the assumption that the gases have a sticking coefficient near 1. Typically, most existing beam systems are conducted in this range so that no clear distinction between the effects of the atomic oxygen and those of other reactive species can be made. What is needed for unambiguous quantitative studies is a pure, well-behaved atomic oxygen beam that has characteristics similar to those experienced in orbit and is operated within a vacuum of 1×10^{-11} torr (with monolayer coverage time of less than 1×10^5 s).

Since the ultrahigh vacuum (UHV) technology for building an appropriate vacuum system is available, efforts are proceeding in the development of an atomic oxygen beam generator with the aforementioned properties. A promising approach uses two unique phenomena. The first is the unusually high permeability of oxygen through silver, which occurs by the sequential adsorption of O_2, surface dissociation into O atoms, dissolution, and subsequent

diffusion of O atoms through a thin Ag membrane or from the bulk of an oxygen-charged Ag sample to a vacuum interface. The second is the use of electron stimulated desorption (ESD) (ref. 3). Normally, when the O atoms arrive at the vacuum interface, surface diffusion occurs and results in O atom collisions and the subsequent desorption of O_2 molecules. If an incident flux of low-energy electrons (E $\approx$ 100 to 500 eV) is directed at this surface, the O atoms are excited to antibonding states before they can recombine and desorb as hyperthermal O neutrals and O^+ ions with an energy of $1 < E < 10$ eV. This paper reports the results of a set of preliminary experiments and serves as a proof of concept of this hypothesis.

Symbols and Abbreviations

AP	appearance potential
CMA	cylindrical mirror analyzer
CN	coordination number
E	kinetic energy, eV
ESD	electron stimulated desorption
ESDIAD	ESD ion angular distribution
ESDIED	ESD ion energy distribution
G_1, G_2	grid designations
I/I_0	current ratio
I_e	current, A
I_{ESD}	electron impact current for ESD, A
k	Boltzmann's constant, $1.38 \times 10^{-23} J\text{-}K^{-1}$
L	langmuir, exposure of 1×10^{-6} torr for 1 s
m/e	ratio of mass to charge, amu
$N(E)$	number of ions
p	pressure, torr
Q	ESD cross section, cm^2
QMS	quadrupole mass spectrometer
T	temperature
t	time, hours
V_{ESD}	electron impact voltage for ESD, V
V_e	voltage, V
γ	recombination coefficient
η	yield
θ	surface coverage
ϕ	molecular flux density, $cm^{-2}\text{-}s^{-1}$

Experiment

Neutral Detection

The schematic of the experimental system employed for detection of neutral O atoms is shown in figure 1. A 0.76-mm-diameter polycrystalline Ag wire (0.99999+ purity) in the shape shown (a hairpin shape provides minimal temperature variation along the straight section) served as the oxygen-charged target. A 0.25-mm-diameter W wire mounted about 2 mm away from and parallel to the Ag wire was used as the electron source. The Ag was cleaned just prior to insertion into the system by ultrasonically cleaning it in detergent for 10 minutes, electropolishing it in a solution of methanol and 6-percent perchloric acid, rinsing it several times in methanol, and immediately drying it with high-purity N_2 gas. Auger electron spectroscopy (AES) shows that only very small amounts of contaminating C, S, and Cl remained on the cleaned surface. These contaminants were removed by successively heating in 10 torr of O_2 at 500°C for 1 hour and then annealing in UHV (ref. 4). The Ag could be resistively heated to as high as 960°C with stepped down line voltage. The temperature of the Ag was measured with a chromel-alumel thermocouple attached to the straight section. Through use of a temperature controller, a prescribed temperature could be attained in less than 10 s. The W filament was also resistively heated and could supply ESD bombardment currents in excess of 10 mA/cm^2. Grid two (G_2) served as an electron repeller, and grid one (G_1) served as a retarding element for positive ions. The ESD assembly was in direct line of sight of a quadrupole mass spectrometer (QMS) located within a UHV environment ($p < 1 \times 10^{-11}$ torr). The QMS data were taken with a minicomputer which was connected to the QMS through a computer interface system. The QMS could be isolated from the UHV chamber by a straight-through valve with an all-metal seal. When this valve is closed, the Ag can be charged with O_2 at pressures in excess of 760 torr without degrading the UHV conditions in the QMS chamber.

The recombination coefficient γ for atomic oxygen on metal is large ($0.01 < \gamma < 1.0$), so its identity changes from reaction with another species (e.g., CO, CO_2, NO, NO_2, N_2O, H_2O, and O_2) in only a few collisions (ref. 5). In order to avoid this problem, the entire ESD assembly was encased in a SiO_2 tube with the open end pointing toward the QMS.

Silicon dioxide has a small recombination coefficient ($\gamma \approx 1 \times 10^{-4}$) and, therefore, provides a more directed and larger atomic oxygen flux toward the QMS. Nevertheless, the flux of unrecombined atomic oxygen is smaller than the flux of recombination products and, hence, difficult to detect. In order to discriminate between the reaction products and those from the other residual gases, the appearance potential (AP) method was adopted. Figure 2 shows the relative intensity of ionization of several gases in a QMS as a function of electron energy. The values of the appearance potentials (from extrapolation to zero intensity) for these gases are consistent with each other and indicate an ion source factor of about 2.5 eV for this instrument. Since the reported appearance potentials for fragmentation of O_2, H_2O, CO, and CO_2 to O^+ are in excess of 16 eV (18.5 V including the ion source factor), operation of the QMS ionizer below this potential will not yield O^+ ions from these other sources (ref. 6). Furthermore, at this voltage the sensitivity to background gases is substantially reduced, thereby giving a directed flux (line of sight from the Ag) which has an enhanced signal-to-background ratio.

While the Ag wire was being charged with oxygen (typical parameters were $p \approx 10$ torr O_2, $T_{Ag} = 500°C$, and $t = 1$ hour), the pressure in the isolated QMS chamber remained below 1×10^{-11} torr. After the wire was charged, the ESD assembly volume was evacuated to about 1×10^{-8} torr and baked out overnight at a temperature of 200°C. During this bakeout period, the Ag was cooled to maintain a temperature below 30°C in order to minimize the O loss. Also, the W filament, G_1, and G_2 were degassed while the ESD assembly volume was hot. After bakeout, the pressure in the ESD assembly volume dropped to 1×10^{-10} torr, at which time the isolation valve was opened and sufficient time was allowed for the entire system to pump down to the 1×10^{-11} torr range. The Ag was then heated to the prescribed temperature and experiments were conducted in both the normal and AP modes.

Ion Detection

The O^+ ion detection and energy distribution measurements were performed in another UHV system (base pressure of 2×10^{-11} torr) with a Ag single crystal with an exposed (110) surface. A schematic diagram of the system is shown in figure 3. In addition to ESD, this system can be used for electron spectroscopy for chemical analysis (ESCA), Auger electron spectroscopy (AES), low-energy-electron diffraction (LEED), temperature-programmed desorption (TPD), and other techniques. The sample was cleaned using Ar ion bombardment followed by annealing at 500°C until AES gave a spectrum corresponding to clean Ag. The clean sample was dosed with 2500 L of O_2 at a pressure of 1.0×10^{-6} torr and room temperature.

The ESD was performed in several different ways with the experimental configuration shown in figure 4. A double-pass cylindrical mirror analyzer (CMA) with an angularly resolving aperture and an internal electron gun was used to perform all the ESD experiments. The electron gun provided an electron beam which could be varied from 100 to 500 eV and from 100 to 20 000 nA over a spot about 0.1 mm in diameter. Four different modes of operation for ESD are possible. (See ref. 4 for a thorough discussion and examples.) The first mode is to continuously perform AES to monitor the O and Ag peak heights as a function of time. This AES yields the total desorption cross section for desorption of ions, neutral atoms, and metastable atoms. The second mode is to obtain a positive ion energy distribution function by sweeping kinetic energy with the energy analyzer. This sweeping collects all positive ions regardless of mass and is referred to as a total ion energy distribution. The third mode yields a mass spectrum of the desorbing ions near a selected ion kinetic energy. This is done with the CMA used as a time-of-flight mass spectrometer. The electron beam is pulsed onto the sample for about 300 ns, and then the ion detection circuitry is time gated with respect to the primary beam that allows mass identification based on flight time. The fourth mode is to scan kinetic energy while time gating the ion signal. This yields an ion kinetic energy distribution for a species with a preselected mass. Two other variables can also be varied easily. The first variable is the primary electron beam energy, which can be varied in any prescribed manner from 50 to 5000 eV. The second variable is the direction of the desorbing ions, which can be varied with the moveable aperture. The first variable is determined from a threshold experiment in which different electronic excitation mechanisms become possible as the primary beam energy increases. The second variable is determined from ESD ion angular distribution (ESDIAD), which has become an important technique for structure determination.

Results

^{16}O Neutral Experiments

Figure 5 shows the residual gas mass spectrum of the ESD assembly after the Ag was charged with $^{16}O_2$ and pumped down to a total pressure of 5×10^{-11} torr. The QMS was in the normal mode (electron energy $V_e = 70$ eV and emission current

I_e = 2.5 mA), and the signal output is plotted in logarithmic form. The spectrum is typical for a clean metal system in the UHV range. The peak at $m/e = 16$ is primarily due to fragmentation of the oxygen-containing residual gases.

Normal mode detection of the thermal desorption (no ESD bombardment current applied) of $^{16}O_2$ from polycrystalline Ag at T_{Ag} = 500°C is presented in figure 6. The desorption temperature was attained within 10 s. Desorption from the surface occurs first and is followed by desorption of bulk oxygen, which diffuses to the surface. The amount of O_2 desorbed plus the oxygen in the oxygen-bearing reaction products at a given time is approximately equal to the total quantity of oxygen desorbed from the Ag.

When ESD conditions of V_{ESD} = 100 V and I_{ESD} = 0.5 mA were applied and with the Ag at 50°C, the CO ($m/e = 28$), CO_2 ($m/e = 44$), and O ($m/e = 16$) peak values immediately increased by a factor of over 100 and the O_2 ($m/e = 32$) peak value increased by a factor of over 200. Figure 7 shows a survey of the many reaction products produced by the atomic oxygen after 20 minutes of operation, that is, H_2O ($m/e = 18$), N_2 + CO ($m/e = 28$), NO ($m/e = 30$), O_2 ($m/e = 32$), CO_2 + N_2O ($m/e = 44$), and NO_2 ($m/e = 46$). The nitrogen-bearing gases were probably produced by displacement of previously pumped N_2 in the Ti of the sublimator and ion pumps with oxygen. This nitrogen was then available for reaction with atomic oxygen. In the AP mode the QMS electron energy was reduced to 18.1 eV (which is effectively about 15.6 eV with the instrument factor), and the emission current was adjusted to 0.62 mA. The ESD parameters used were the same as previously indicated, and the Ag temperature was elevated to T_{Ag} = 300°C. A mass survey from 0 to 50 amu was then taken and is shown in figure 8. The atomic oxygen is clearly evident in this scan. When the Ag temperature was reduced, the $^{16}O^+$ signal decreased and ultimately was not detected below T_{Ag} = 100°C. Gas phase and ESD positive ions created by the electron flux were retarded by G_1 and were not studied, since the signal-to-noise ratio (ratio of ESD ions to gas phase ions) was very near 1.0. These conditions indicate that the O^+ signal obtained in the ESD experiment was due to ionization of neutral atoms desorbing from the Ag surface. Since the residual gas pressure in the system was 10^{-10} torr during the ESD experiments, the lower sensitivity of the AP mode would require background pressures over two orders of magnitude higher to be detectable on this scale. In figure 8, there is also an atomic hydrogen (H) signal that is from ESD. The source is probably from dissolved hydrogen since the solubility and diffusivity are very high for hydrogen in Ag (ref. 7).

Although the appearance potential of O_2 is only 12 V as compared with 14 V for O (O_2 therefore having a higher sensitivity), its absence from the spectra indicates that O from ESD is the predominant species desorbed at this temperature. Interestingly, O_2 is only detectable in the AP mode when its concentration in the Ag is very high and the Ag temperature is above 500°C. These data are shown in figure 9. Since the concentration of oxygen in the Ag wire was continuously decreasing, the $^{16}O_2$ signal from ESD also decreased with time, but relatively slowly, since the flux of O to the surface was sufficient to keep the atomic surface coverage high ($\theta \approx 0.5$). Furthermore, as the Ag temperature increased, the rate of oxygen diffusing from the Ag bulk to the Ag surface increased the surface concentration and ESD O flux. Both of these phenomena are shown in figures 10 and 11. Experiments were also conducted which verify the linear increase in ESD flux with increasing bombardment current.

^{18}O Neutral Experiments

Similar ESD experiments were run after the Ag wire was charged with $^{18}O_2$. As shown in figure 12, ^{18}O is detected if the Ag temperature is maintained at 200°C and the QMS is operated in the AP mode. The Ag had not been fully depleted of ^{16}O from previous experiments, so a significant peak at $m/e = 16$ remains. The fact that it is larger than the ^{18}O peak is probably due to both the extensive desorption of ^{16}O bearing gases from the chamber surfaces and the residual ^{16}O diffusing from the subsurface region. At higher temperatures, the linear temporal decrease in ^{16}O signal occurred much faster than the ^{18}O signal decrease, so that ^{18}O ultimately became the dominant species. Figure 13 shows a mass survey spectrum taken in the AP mode at T_{Ag} = 450°C. In this case, the ^{18}O peak has become dominant. Results of experiments run in the AP mode which demonstrate the variation in ^{18}O signal with primary electron beam energy are presented in figure 14. The ^{18}O signal apparently disappeared at an energy of approximately 35 eV, which set an upper limit for the ESD threshold of oxygen adsorbed on Ag. As indicated above, the ESD of ^{18}O from polycrystalline Ag depended upon the concentration of surface oxygen and was controlled by the diffusion flux to the surface. Allowing Ag to remain at 450°C for several minutes without electron bombardment and then reducing the temperature to 100°C provided a surface coverage of about 0.5. Electron stimulated desorption on this surface yielded an ^{18}O signal

decay rate which was indicative of desorption from the surface with no diffusion of ^{18}O to the surface. These data are presented in figure 15 and can be used to determine the ESD cross section for desorption of O.

O^+ Experiments

Experimentally, an energy distribution for the desorbing neutral oxygen atoms is exceedingly difficult to obtain. However, since ions and neutral atoms are both produced through decay of the same electronic excitations (ref. 4), one can reasonably assume that the energy distributions of the desorbing ions and neutral atoms are very similar.

Following a 2500-L room-temperature dose of oxygen, two desorption energies for O^+ were observed, one at 2.4 eV and a second at 5.4 eV. These two desorption energies may indicate the presence of at least two binding sites for oxygen on Ag(110) at 0°C. A marked effect in the relative desorption yields from these two states is observed upon excitation of the Ag 3*d* core levels binding energies of $3d_{3/2}$ = 361.9 and $3d_{5/2}$ = 367.9. This effect is shown in figure 16. Shown in parts A and B of figure 16 are two energy distribution curves obtained consecutively from the same position on the sample surface. A primary beam energy of 300 eV was used to obtain part A of figure 16 and a beam energy of 400 eV was used for part B of figure 16. The same procedure used to obtain parts A and B of figure 16 was used to obtain parts C and D, but the 400-eV spectrum of part C was taken prior to the 300-eV spectrum of part D. These spectra clearly show that upon exciting the Ag 3*d* core levels the 5.4-eV emission feature yield decreases sharply with respect to that of the 2.4-eV feature.

Preliminary angle-resolved (ESDIED-ESDIAD) spectra shown in figure 17 not only support the premise that there are two binding states present but also show that they desorb predominantly at different angles. At a near-normal desorption angle with respect to the surface plane, the state with a 5.4-eV desorption energy is more prominent (part B of fig. 17), whereas in the angle-integrated spectrum, the state with a 2.4-eV desorption energy is more prominent (part A of fig. 17).

Discussion

Desorption Analysis

The straight section of the Ag wire can be approximated as a long cylinder of length ℓ and diameter d. The variation of the concentration of oxygen in this geometry as a function of time can be represented by the solution to Fick's second law for finite cylinders desorbing into a vacuum (surface concentration is zero) (ref. 8):

$$\frac{C}{C_o} = \frac{32}{\pi^2} \sum_{n=0}^{\infty} \frac{\exp[-(2n+1)^2\pi^2 Dt/\ell^2]}{(2n+1)^2} \times \sum_{n=1}^{\infty} \frac{\exp\left(-4\beta_n^2 Dt/d^2\right)}{\beta_n^2} \tag{1}$$

where C is the average concentration in the solid at t, C_o is the initial concentration in the solid, β_n is the root of $J_0(\beta) = 0$, and D is the diffusion coefficient. After a short interval of time t_o, the two series may be reduced to their first terms so that

$$\frac{C}{C_o} = \frac{32}{\pi^2\beta_1^2} \exp[-t/\tau] \quad (t > t_o) \tag{2}$$

where

$$\frac{1}{\tau} = \left(\frac{\pi^2}{\ell^2} + \frac{4\beta_1^2}{d^2}\right) D$$

The total amount of gas desorbed into the vacuum per unit volume of the wire after time t is just $C_o - C$, so the desorbing flux is then

$$\phi_o(t) = -\frac{dC}{dt} = -\frac{32C_o}{\pi^2\beta_1^2\tau} \exp\,(-t/\tau) \tag{3}$$

Now the rate of change of pressure p in the system caused by the influx of oxygen from the Ag (and the simultaneous pumping speed S through the mass spectrometer) is

$$V\frac{dp}{dt} = \phi_o(t) - S(p - p') \tag{4}$$

where V is the volume of the ESD chamber and p' is the pressure in the lower chamber. Since $p >> p'$ for all t and $\phi_o(t)$ is defined by equation (3), then

$$\frac{dp}{dt} + \frac{1}{\tau'}\, p = A \exp(-t/\tau) \tag{5}$$

where

$$\tau' = \frac{V}{S} \quad \text{and} \quad A = \frac{-32C_o}{\pi^2\beta_1^2\tau V}$$

Equation (5) has the solution

$$p = A\left(\frac{\tau'\tau}{\tau - \tau'}\right)[\exp(-t/\tau) - \exp(-t/\tau')] \tag{6}$$

which is the pressure variation with time. The known values of the volume of the ESD chamber and the pumping speed indicate that even for unusually high

values of D (which means τ is small), $\tau >> \tau'$ and therefore $\exp(-t/\tau) >> \exp(-t/\tau')$, so equation (6) becomes

$$p \approx A\tau' \exp(-t/\tau) \tag{7a}$$

or

$$\log p \approx \log A\tau' - \frac{t}{2.3\tau} \tag{7b}$$

The slope of a log p versus t plot thus yields the diffusion coefficient, since

$$D = \frac{2.3m}{(\pi^2/\ell^2) + (4\beta_1^2/d^2)} \tag{8}$$

where m is the slope. The average concentration of oxygen in the Ag can be determined from integration of equation (4) over the desorbing interval τ. This integration yields

$$C = \frac{2S}{VkT} \int_\tau p(t)\, dt \tag{9}$$

where T is the temperature of the system.

Surface Properties

The interaction between oxygen and a Ag surface has received much attention, mainly because of the high activity of Ag for the selective epoxidation of ethylene. The bulk of the present understanding of this system has been derived from studies of oxygen adsorption on the (100), (110), and (111) single-crystal surfaces of Ag (refs. 9 to 28). The inconsistencies among these studies clearly indicate that chemically bound oxygen on Ag is not well understood presently. These discrepancies seem to arise from the various oxygen exposure conditions used. The results of these studies are described briefly for each surface.

O/Ag(100). This surface is the least researched of the three. The sticking coefficient for oxygen on this surface is on the order of 10^{-5} to 10^{-6}. Based on work function measurements, the existence of two binding states of oxygen on this surface has been tentatively proposed (ref. 9): one state which exists alone at temperatures above 97°C and a second state which increases in relative concentration with decreasing temperature. Oxygen exposure causes a decrease in the spot intensity of the 1×1 low-energy-electron diffraction (LEED) pattern of the clean surface. The appearance of new diffraction spots upon oxygen adsorption is a controversial topic. Two observations have been presented in the literature. One observation is that new diffraction spots appear, an occurrence which suggests that adsorption is either disordered or in a phase with a 1×1 structure. The second observation is that oxygen adsorption causes facets of the (410) plane to form which are inclined 14° relative to the (100) surface domains (ref. 21). Thermal desorption of adsorbed oxygen from this surface occurs near 240°C.

O/Ag(110). The (110) surface is the most reactive toward oxygen with an initial sticking coefficient of approximately 10^{-3}. The initial sticking coefficient decreases with increasing temperature, an occurrence which may provide evidence for a precursor state for chemisorption of oxygen. Based on LEED patterns obtained with various exposures for a room-temperature oxygen exposed (110) surface, the maximum surface coverage is proposed to be half a monolayer. In addition to the precursor state, three adsorbed states of oxygen have been proposed: an adsorbed dioxygen state, an adsorbed dissociated oxygen state, and a subsurface dissociated oxygen state. The dioxygen state has been most commonly observed at temperatures below −153°C and produces a diffraction pattern which indicates a 1×1 structure. It has also been proposed that a dioxygen adsorbed state exists at 200°C following oxygen exposures at or exceeding 0.1 torr. However, it is not clear presently if these dioxygen states are the same. The dissociated oxygen state is formed by exposure at temperatures equal to or greater than −103°C or by heating an already exposed surface above −103°C. This state is the most prominent adsorbed state of oxygen above −103°C, and the binding site is unknown. None of the bonding models proposed to date take into account probable adsorbate-induced surface reconstruction nor are they consistent with the available data. The subsurface dissociated oxygen is formed by either heating an oxygen-exposed surface above 147°C or by dosing at temperatures above 147°C. This subsurface oxygen is stable to 327°C. Above 327°C the surface and subsurface oxygen atoms combine and desorb as O_2. It has also been suggested that this subsurface oxygen migrates to the surface near 267°C.

O/Ag(111). The (111) surface is similar in reactivity toward oxygen to the (100) surface in that it has a sticking coefficient on the order of 10^{-6}. At temperatures below −123°C the prominent surface species is O_2, which desorbs near −58°C. Above this temperature the adsorbed state of oxygen is controversial. It is not clear whether an adsorbed dioxygen species exists above −58°C. An exposure of 1 to 2 torr of oxygen in the range of 127°C to 227°C results in a diffraction pattern with a $p(4 \times 4)$ structure. This structure is stable to approximately 307°C,

where it associatively desorbs as O_2. As for the (110) surface, a subsurface state is proposed which desorbs above 327°C.

Polycrystalline Ag may contain all the binding states associated with the crystalline surfaces described above. In addition, states which may be associated with grain boundaries and other defects could be important. Therefore, studies of single-crystal surfaces may only offer a general indication of the behavior of a polycrystalline surface. In agreement with the single-crystal studies, 497°C is sufficient for desorption of all the surface oxygen to occur. No surface-controlled phenomena appear to limit the thermal evolution of oxygen from the surface.

O/Ag Diffusion

The diffusivity of ^{16}O in polycrystalline Ag at $T_{Ag} = 500°C$ was determined from equation (8) and the slope of the $^{16}O_2$ curve in figure 6 and was found to be 2.64×10^{-6} cm^2-s^{-1}. This value compares very well with the results of Eichenauer and Mueller (ref. 7) and of Ramanarayanan and Rapp (ref. 29). An estimate of the oxygen flux arriving at the surface from the Ag bulk can now be made through use of equation (3). If we assume the value of C_o to be that of the solubility limit of Ag at 500°C and p = 10 torr, the $^{16}O_2$ charging condition would give a bulk concentration of 2.7×10^{17} O atoms-cm^{-3} Ag. A flux of 3.18×10^{13} atoms-cm^{-2}-s^{-1} has been determined in this study. Taking the average number of sites for polycrystalline Ag as 1.3×10^{15} atoms-cm^{-2}, this value of ϕ_o corresponds to formation of a monolayer ($\theta = 0.5$) in approximately 20 s, but after about 3 minutes the evolving flux decreased by an order of magnitude. At 300°C, however, $\phi(t)$ had not decreased an order of magnitude until 60 minutes had transpired. Since the 300°C temperature is just below the thermal desorption temperature of the surface and subsurface oxygen, the desorbing O/O_2 ratio is maximized (ref. 13).

ESD Analysis

The total number of desorbing particles, including neutral and metastable atoms i, positive ions i^+, and negative ions i^-, can be represented by

$$I = i + i^+ + i^- \tag{10}$$

The total cross section Q for ESD is defined by

$$\frac{I}{A_\varepsilon} = \frac{I_e}{A_\varepsilon} QN \tag{11}$$

where I_e is the total electron beam current to the sample, A is the area of the sample bombarded, ε is the charge of the electron, and N is the surface concentration of the chemisorbed species. The change in surface concentration as a function of time is

$$-\frac{dN}{dt} = \frac{I_e}{A_\varepsilon} QN \tag{12}$$

which integrates to

$$\frac{N}{N_o} = \exp\left(-\frac{I_e}{A_\varepsilon} Qt\right) \tag{13}$$

where N_o is the initial surface concentration of the chemisorbed species. If N can be measured as a function of time with some surface diagnostic technique, then Q can be determined from equation (13) if I_e and A are known.

In this case, if we assume a direct correlation between the flux leaving and the change in surface concentration and that neutral atoms are the predominant desorbing species, the neutral atom cross section Q_n can be determined from

$$\frac{i}{i_o} = \frac{N}{N_o} = \exp\left(-\frac{I_e}{A_\varepsilon} Q_n t\right) \tag{14}$$

The term Q_n is calculated from the decay in ^{16}O and ^{18}O signals, such as those shown in figure 15. The values obtained vary from 5.6×10^{-19} to 8.9×10^{-19} cm^2, with an average value of 7×10^{-19} cm^2 for five runs at a temperature of 450°C. The values for ^{16}O and ^{18}O do not appear to be significantly different; therefore, very little isotope effect is shown, as expected (ref. 4). These values compare well with ESD cross sections of metal systems studied previously (refs. 30 and 31). With this average cross section, the yield is $\eta = 7 \times 10^{-4}$ atoms per electron, and the flux of O atoms leaving the Ag surface as a result of ESD ($\theta = 0.5$) is

$$\phi_o = \eta\phi_e = 1.1 \times 10^{12} \text{ cm}^{-2}\text{-s}^{-1}$$

For the geometry of the ESD system and the directionality of the ESD atoms (most appear to be axial), it is estimated that about 20 percent of the O atoms reach the ion source of the QMS without recombining after leaving the fused SiO_2 tube. Furthermore, an effective pumping speed S through the QMS of about 4 liters per second maintains an equivalent pressure in the ion source of about 1.7×10^{-9} torr. The sensitivity of the QMS for O is assumed to be approximately the same as for O_2, which has been measured in the AP mode to be 5×10^{-3}A-torr^{-1} and results in an ion current of about 1×10^{-11}A. This current level is consistent with the level of O signal detected in the AP mode.

It is unclear what effect the flux of O atoms arriving at the surface from the bulk has on the atomically bonded surface atoms, but it is plausible that the subsurface state is filled (at elevated temperatures) since the ^{18}O isotope experiments demonstrate that there is a rapid exchange of atoms to and from the surface. Therefore, surface atoms lost by ESD are immediately replaced from those in the subsurface. Below 450°C most atoms desorb by ESD rather than by thermal desorption. This is in good agreement with Backx, De Groot, and Biloen, who found that on the (110) face the subsurface oxygen is stable below 450°C (ref. 11). It has been suggested that oxygen adsorbed in high-symmetry, high-coordination states does not yield significant O^+ ESD signals, whereas O adsorbed at step edges or sites of reduced coordination produces much higher yields. Bange, Madey, and Sass have shown that O does not bond in the troughs on a (110) face (CN = 4) but at a polar angle of 12° along [001] azimuths where CN = 1 or, perhaps at most, CN = 2 (ref. 32). Furthermore, there may also be a surface reconstruction that takes place in which Ag atoms move from their normal lattice points. Bange, Madey, and Sass have noted from ESDIAD data that the angle of the desorbed ions varies with surface temperature and that this variation may be indicative of some type of surface reconstruction (ref. 32). Finally, there may also be a significant minority state contribution because of paths of diffusion from the bulk, such as grain boundaries, dislocations, and twin boundaries. Since oxygen adsorbed at these sites would have lower coordination numbers, this oxygen group probably contributes significantly to the ESD flux.

A possible interpretation of the energy distribution of the O^+ ions involves an interatomic Auger transition. One deexcitation mode of a Ag 3*d* hole is a core-valence-valence (CVV) Auger transition. This transition results in the two most notable features in the Ag Auger spectrum, which are found at kinetic energies of 351 and 356 eV. When oxygen is adsorbed on Ag, one or both of the valence electrons involved in this Auger transition may be associated with the oxygen. Furthermore, an interatomic transition may be expected because the valence levels of Ag in silver oxide are associated with a filled 4*d* shell, and thus silver oxide might be considered to be an ionic material with quasi-maximal valency. Interatomic Auger transitions have been observed in the maximal valency oxides of Ti, V, and Mn (ref. 33) and have been proposed to result in the ESD of O^+ ions (ref. 34). Through comparison of curves in figure 16, it is evident that the state which desorbs at 5.4 eV is depleted when the 400-eV primary beam is used. The 5.4-eV shoulder in part C of figure 16 is less prominent than this shoulder in part A, which is suggested to be a result of the 400-eV primary beam spectra being taken first. This depletion of the 5.4-eV state may be caused by an interatomic transition between Ag and oxygen, resulting in a transformation of oxygen in the state which desorbs at 5.4 eV to the state which desorbs at 2.4 eV.

It is also possible that the two desorption energies for O^+ are derived from the same adsorption state but from different desorption mechanisms. This, however, seems unlikely. Exposure of the surface to a 400-eV electron beam before the acquisition of an energy distribution with a 300-eV primary beam yields a reduction in the number of desorbing ions with a kinetic energy of 5.4 eV compared with that obtained without exposing the surface to a 400-eV beam. A mechanistic change would not be expected upon preexposing the surface to a 400-eV electron beam; thus, an adsorbate state change must have occurred.

The neutral-atom experiments indicate that another threshold exists below a primary electron beam energy of 35 eV. Since the signal becomes very small at low primary beam energies, it is quite possible that this threshold actually occurs at about 26 eV, which is the energy required to create a core hole in the high-lying O 2*s* level. Decay of this core hole would then lead to desorption of oxygen, but the electronic deexcitation responsible for decay is not currently understood.

The O/Ag chemisorption system is clearly very complex. Furthermore, ESD of oxygen yields results which strongly depend upon a large number of variables, including primary electron beam energy, sample temperature, surface morphology, oxygen coverage, and direction of desorption. Although much effort is required to characterize this behavior, this system allows much flexibility for attaining properties desirable in the functioning of an oxygen atom beam system.

Concluding Remarks

The generation of atomic oxygen by electron stimulated desorption from dissolved oxygen diffusing to a silver surface is shown to be possible. Polycrystalline Ag charged with $^{16}O_2$ and $^{18}O_2$ and bombarded by low-energy electrons (≈100 eV) under ultrahigh vacuum conditions emits O atom flux levels of 1×10^{12} cm^{-2}-s^{-1} at a Ag temperature of 300°C. The neutral-atom cross section is approximately 7×10^{-19} cm^2. Ancillary experiments conducted on Ag(110) single crystals that have been

dosed with 2500 L of $^{16}O_2$ show O^+ desorption with a mean energy distribution of 2 to 6 eV. There is also some evidence for directionality of the emitted flux, since both the O and O^+ experiments give this indication. On the basis of this research, it appears that the proof of concept has been demonstrated and that the development of an instrument suitable for simulation of the gaseous orbital environment encountered by an orbiting body is feasible.

NASA Langley Research Center
Hampton, Virginia 23665-5225
February 4, 1987

References

1. Leger, L. J.; Visentine, J. T.; and Kuminecz, J. F.: Low Earth Orbit Atomic Oxygen Effects on Surfaces. AIAA-84-0548, Jan. 1984.
2. Outlaw, R. A.; and Brock, F. J.: Orbiting Molecular-Beam Laboratory. *J. Vac. Sci. & Technol.*, vol. 14, no. 6, Nov./Dec. 1977, pp. 1269–1275.
3. Hoflund, Gar B.: A Review of Electron Stimulated Desorption (ESD) Phenomena: Energy Analysis of Desorbing Ions. *Scanning Electron Microsc.*, vol. 1985, part IV, Dec. 1985, pp. 1391–1420.
4. Rovida, G.; Pratesi, F.; Maglietta, M.; and Ferroni, E.: Chemisorption of Oxygen on the Ag(111) Surface. *Surf. Sci.*, vol. 43, no. 1, May 1974, pp. 230–256.
5. Melin, Gerald A.; and Madix, R. J.: Energy Accommodation During Oxygen Atom Recombination on Metal Surfaces. *Trans. Faraday Soc.*, vol. 67, pt. 1, no. 577, Jan. 1971, pp. 198–211.
6. Franklin, J. L.; Dillard, J. G.; Rosenstock, H. M.; Herron, J. T.; Draxl, K.; and Field, F. H.: *Ionization Potentials, Appearance Potentials, and Heats of Formation of Gaseous Positive Ions.* NSRDS-NBS 26, U.S. Dep. Commerce, June 1969.
7. Eichenauer, Walter; and Mueller, Gudrun: Diffusion and Solubility of Oxygen in Silver. *Z. Met.kd.*, Bd. 53, 1962, pp. 321–324.
8. Hill, M. L.; and Johnson, E. W.: The Diffusivity of Hydrogen in Nickel. *Acta Met.*, vol. 3, no. 6, Nov. 1955, pp. 566–571.
9. Engelhardt, H. A.; and Menzel, D.: Adsorption of Oxygen on Silver Single Crystal Surfaces. *Surf. Sci.*, vol. 57, no. 2, July 1976, pp. 591–618.
10. Barteau, M. A.; and Madix, R. J.: The Adsorption of Molecular Oxygen Species on Silver (110). *Surf. Sci.*, vol. 97, no. 1, 1980, pp. 101–110.
11. Backx, C.; De Groot, C. P. M.; and Biloen, P.: Adsorption of Oxygen on Ag(110) Studied by High Resolution ELS and TPD. *Surf. Sci.*, vol. 104, no. 1, Mar. 1981, pp. 300–317.
12. Grant, R. B.; and Lambert, R. M.: Basic Studies of the Oxygen Surface Chemistry of Silver: Chemisorbed Atomic and Molecular Species on Pure Ag(111). *Surf. Sci.*, vol. 146, no. 1, Oct. 1981, pp. 256–268.
13. Campbell, Charles T.: Atomic and Molecular Oxygen Adsorption on Ag(111). *Surf. Sci.*, vol. 157, no. 1, July 1985, pp. 43–60.
14. Puschmann, A.; and Haase, J.: Surface EXAFS of the (2×1) Oxygen Adlayer on Ag(110). *Surf. Sci.*, vol. 144, nos. 2/3, Sept. 1984, pp. 559–566.
15. Eickmans, J.; and Otto, A.: The Transition From Physisorbed to Chemisorbed Oxygen on Silver Films Studied by Photoemission. *Surf. Sci.*, vol. 149, no. 1, Jan. 1985, pp. 293–312.
16. Peuckert, M.: On the Adsorption of Oxygen and Potassium Hydroxide on Silver. *Surf. Sci.*, vol. 146, nos. 2/3, Nov. 1984, pp. 329–340.
17. Bange, K.; Madey, T. E.; and Sass, J. K.: Characterization of OH(ad) Formation by Reaction Between H_2O and O(ad) on Ag(110). *Surf. Sci.*, vol. 152/153, pt. 1, Apr. 1985, pp. 550–558.
18. Prince, K. C.; and Bradshaw, A. M.: Valence Level Photoelectron Spectroscopy of the Oxygen and Carbonate Species on Silver (110). *Surf. Sci.*, vol. 126, nos. 1–3, Mar. 1983, pp. 49–57.
19. Au, Chak-Tong; Singh-Boparai, Sunder; Roberts, M. Wyn; and Joyner, Richard W.: Chemisorption of Oxygen at Ag(110) Surfaces and Its Role in Adsorbate Activation. *J. Chem. Soc., Faraday Trans. 1*, vol. 79, 1983, pp. 1779–1791.
20. Sporken, R.; Thiry, P. A.; Pireaux, J. J.; Caudano, R.; and Adnot, A.: Work Function Measurements With a High Resolution Electron Energy Loss Spectrometer: Application to the Interaction of Oxygen With Ag(110). *Surf. Sci.*, vol. 160, no. 2, Sept. 1985, pp. 443–450.
21. Rovida, G.; Pratesi, F.; Maglietta, M.; and Ferroni, E.: Effects of Oxygen on Silver Surface Structure. *J. Vac. Sci. & Technol.*, vol. 9, no. 2, Mar./Apr. 1972, pp. 796–799.
22. Prince, K. C.; Paolucci, G.; Bradshaw, A. M.; Horn, K.; and Mariani, C.: Oxygen Adsorption on Ag(110): Observation of a Precursor State. *Vacuum*, vol. 33, nos. 10–12, Oct.–Dec. 1983, p. 867.
23. Kagawa, S.; Iwamoto, M.; Morita, S.; and Seiyama, T.: Isotopic Study of the Temperature-Programmed Desorption of Oxygen From Silver. *J. Chem. Soc., Faraday Trans. 1*, vol. 78, 1982, pp. 143–146.
24. Rovida, G.; and Pratesi, F.: Chemisorption of Oxygen on the Silver (110) Surface. *Surf. Sci.*, vol. 52, no. 3, Nov. 1975, pp. 542–555.
25. Goddard, P. J.; and Lambert, R. M.: Basic Studies of the Oxygen Surface Chemistry of Silver: Oxygen, Dioxygen, Oxide and Superoxide on Rubidium-Dosed Ag(111). *Surf. Sci.*, vol. 107, nos. 2/3, June 1981, pp. 519–532.
26. Heiland, W.; Iberl, F.; Taglauer, E.; and Menzel, D.: Oxygen Adsorption on (110) Silver. *Surf. Sci.*, vol. 53, Dec. 1975, pp. 383–392.
27. Zanazzi, E.; Maglietta, M.; Bardi, U.; Jona, F.; and Marcus, P. M.: Test of Structural Models for Ag(110) 1×2–0 by LEED Intensity Analysis. *J. Vac. Sci. & Technol.*, vol. 1, no. 1, Jan.–Mar. 1983, pp. 7–11.
28. Joyner, R. W.; and Roberts, M. W.: A Study of the Adsorption of Oxygen on Silver at High Pressure by Electron Spectroscopy. *Chem. Phys. Lett.*, vol. 60, no. 3, Jan. 15, 1979, pp. 459–462.
29. Ramanarayanan, T. A.; and Rapp, R. A.: The Diffusivity and Solubility of Oxygen in Liquid Tin and Solid Silver and the Diffusivity of Oxygen in Solid Nickel. *Metall. Trans.*, vol. 3, no. 12, Dec. 1972, pp. 3239–3246.
30. Madey, Theodore E.; and Yates, John T., Jr.: Electron-Stimulated Desorption as a Tool for Studies of Chemisorption: A Review. *J. Vac. Sci. & Technol.*, vol. 8, no. 4, July/Aug. 1971, pp. 525–555.
31. Madey, Theodore E.: The Role of Steps and Defects in Electron Stimulated Desorption: Oxygen on Stepped

W(110) Surfaces. *Surf. Sci.*, vol. 94, nos. 2/3, Apr. 1980, pp. 483–506.

32. Bange, K.; Madey, T. E.; and Sass, J. K.: The Adsorption of Oxygen on Ag(110): A New View of Structure and Bonding. *Chem. Phys. Lett.*, vol. 113, no. 1, Jan. 4, 1985, pp. 56–62.
33. Rao, C. N. R.; and Sarma, D. D.: Interatomic Auger Transitions in Transition-Metal Oxides. *Phys. Rev. B.*, vol. 25, no. 4, Feb. 15, 1982, pp. 2927–2929.
34. Knotek, Michael L.: Stimulated Desorption From Surfaces. *Phys. Today*, vol. 37, no. 9, Sept. 1984, pp. 24–32.

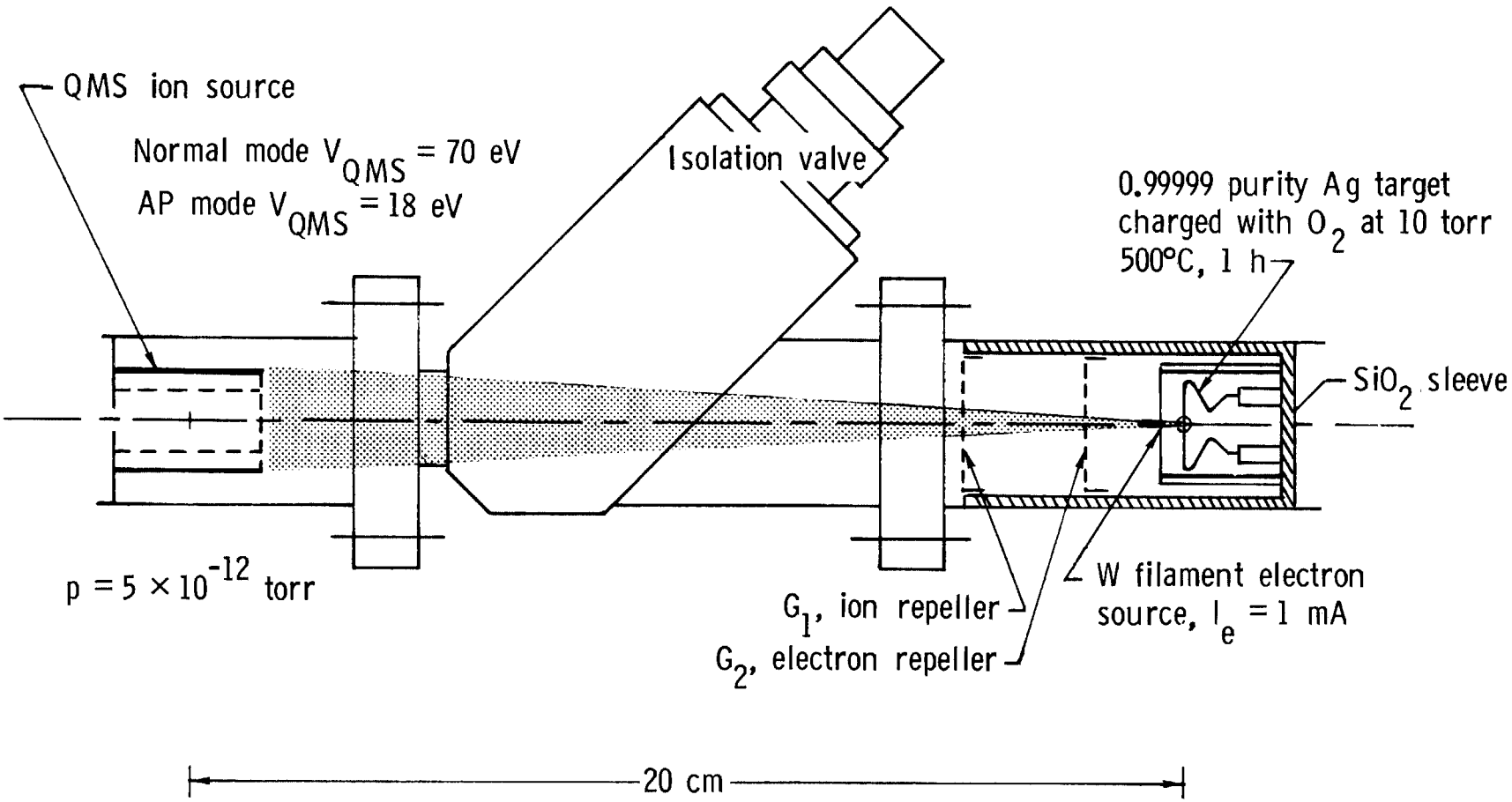

Figure 1. Schematic diagram of ESD apparatus.

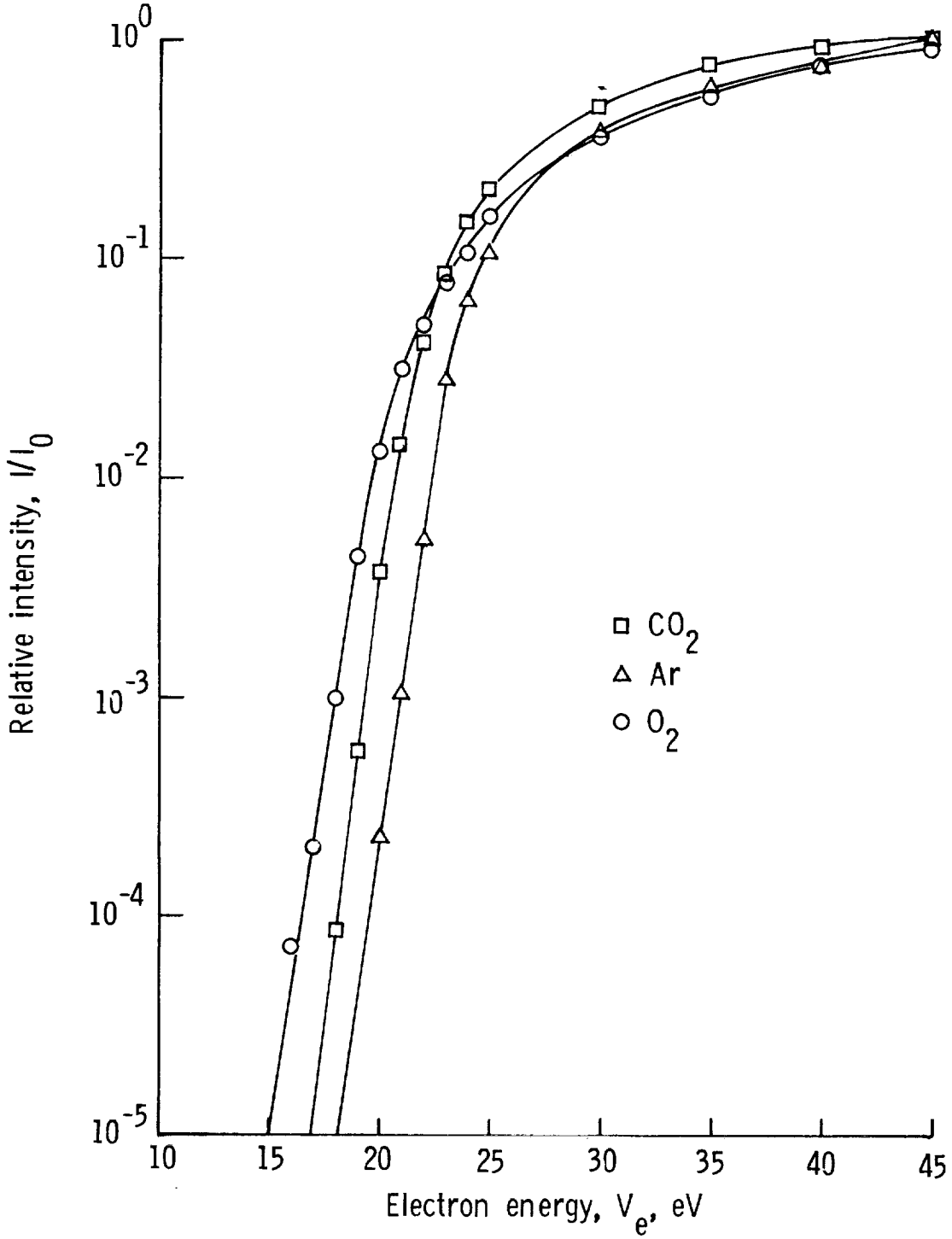

Figure 2. Appearance potential curves for several gases. $I_e = 0.5$ mA; $p = 2 \times 10^{-8}$ torr.

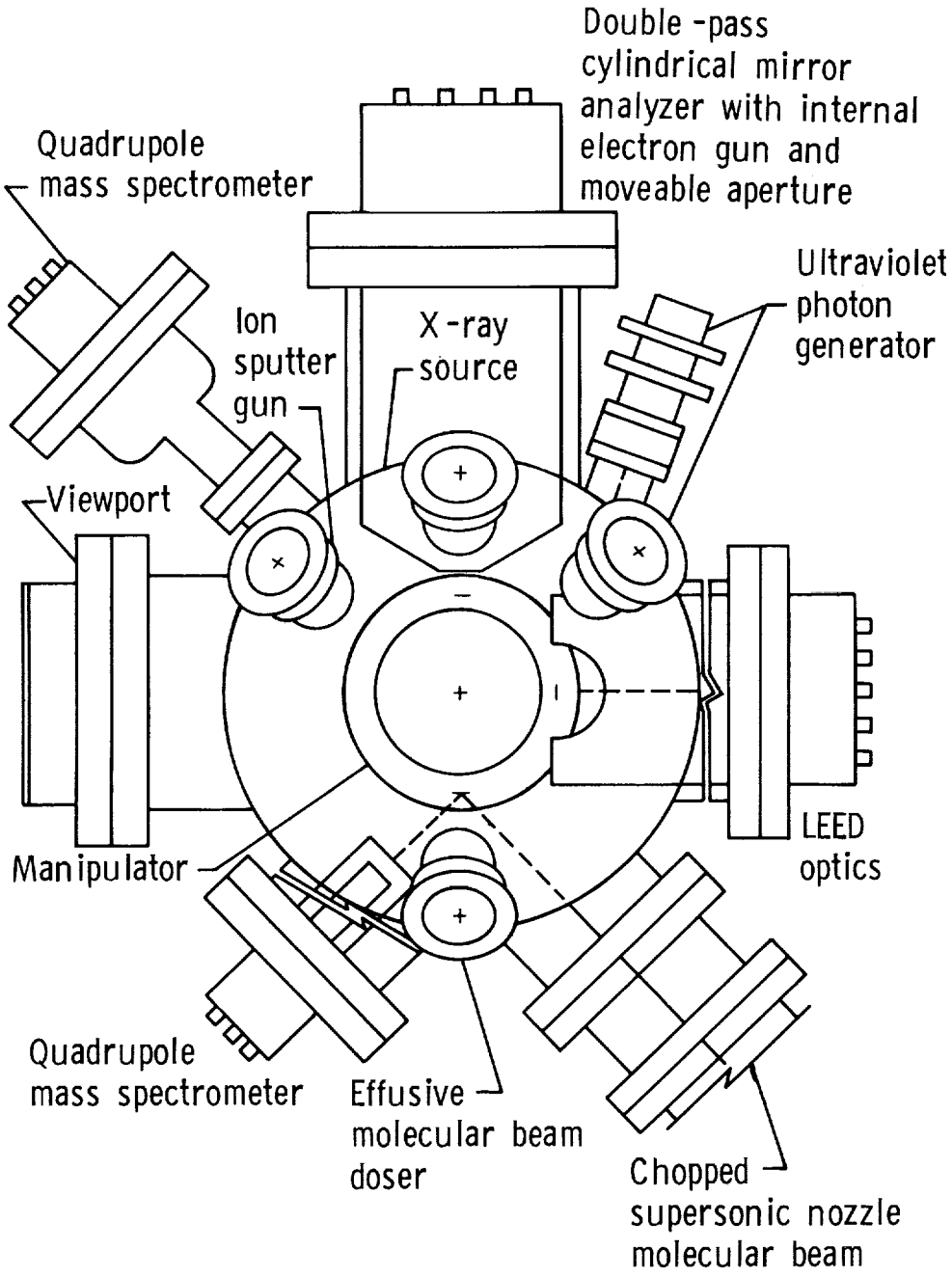

Figure 3. Schematic diagram of surface analysis system used for ESD and surface characterization studies.

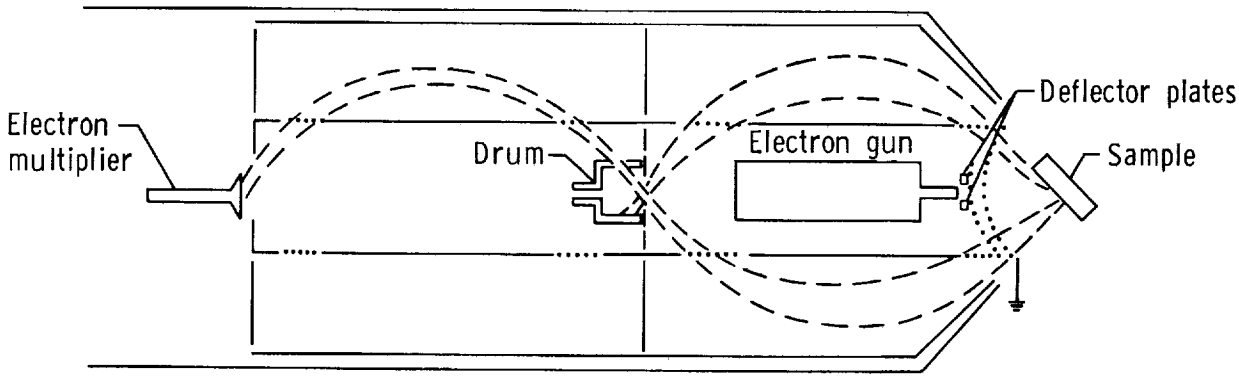

Figure 4. Schematic diagram of cylindrical mirror analyzer (CMA) used for ESD.

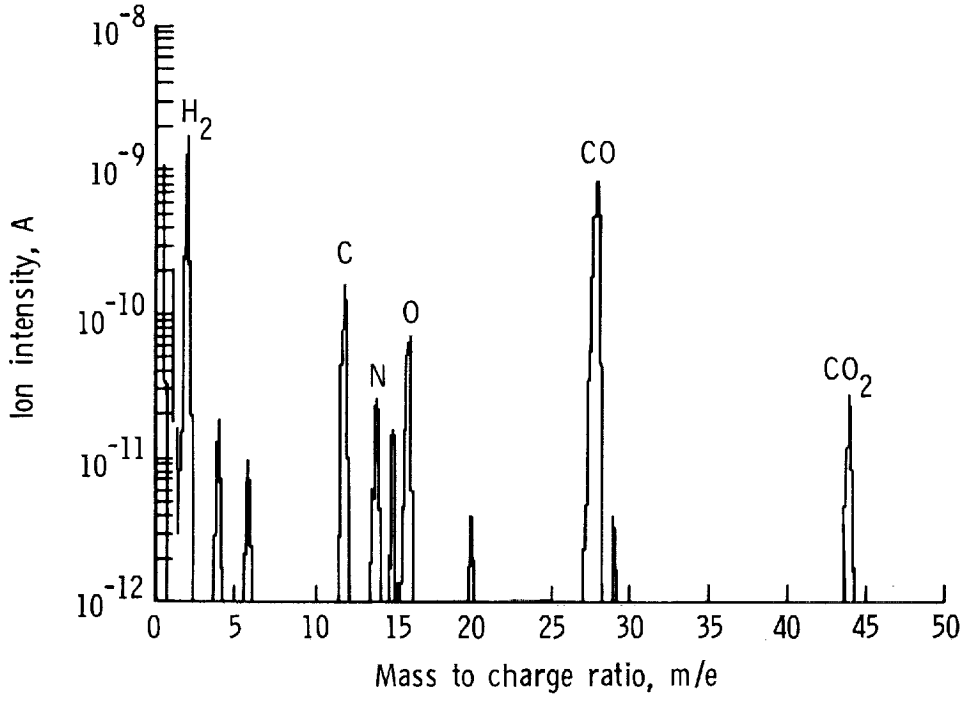

Figure 5. Prerun mass survey for Ag charged with $^{16}O_2$ (normal QMS operating mode). $p = 5 \times 10^{-11}$ torr.

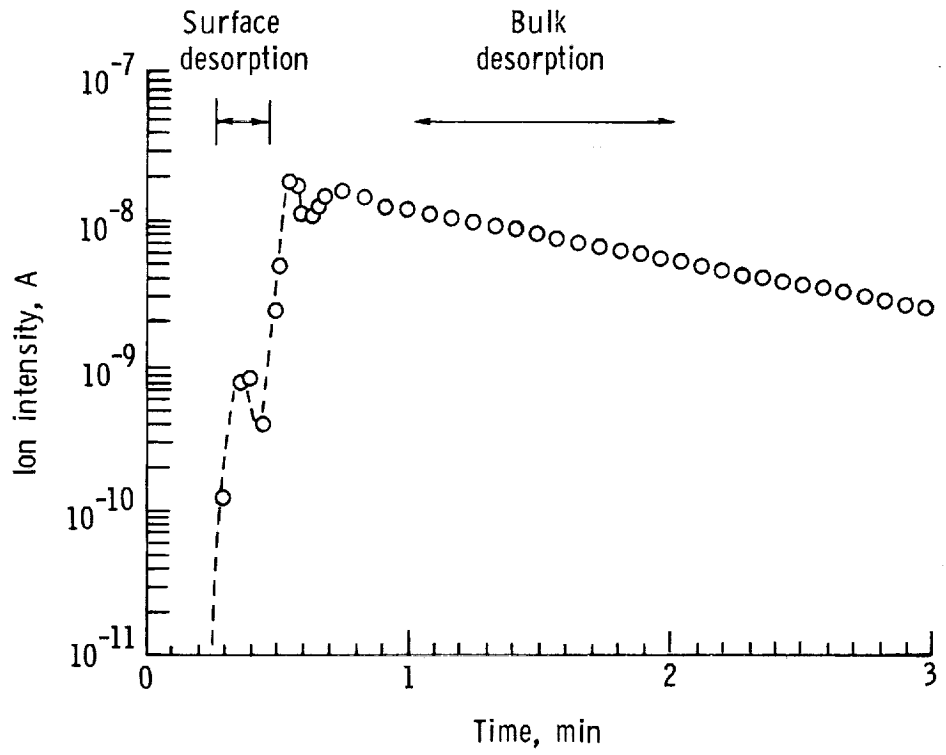

Figure 6. Desorption of $^{16}O_2$ as a function of time (normal QMS operating mode). Note linear decay of the signal on the log plot. $T_{Ag} = 500°C$.

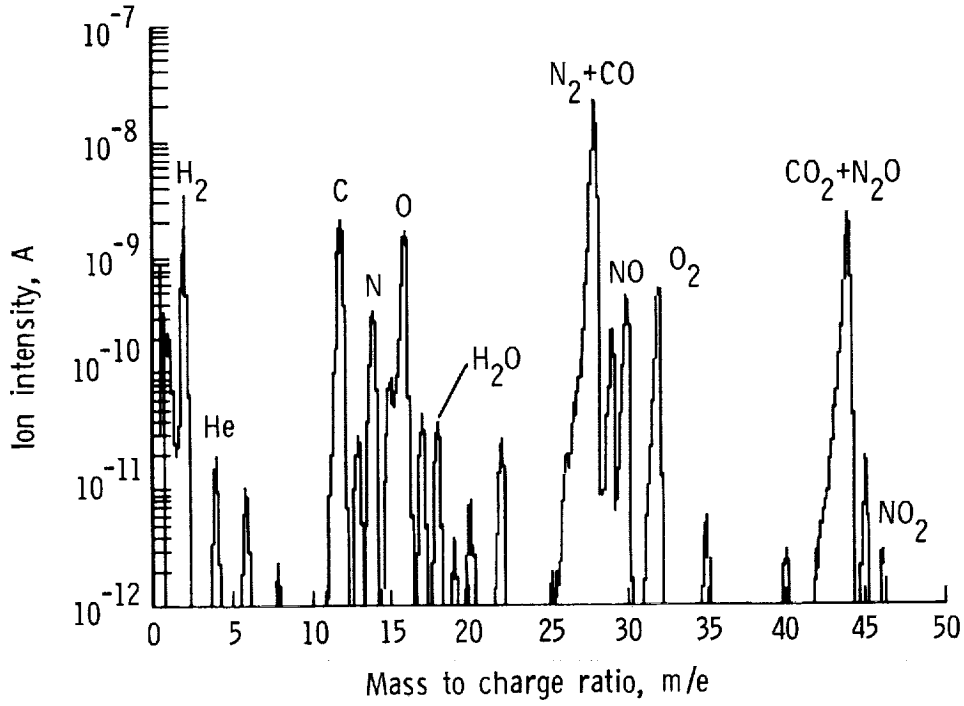

Figure 7. Mass survey of atomic oxygen reaction products after 20 minutes of ESD (normal QMS operating mode).

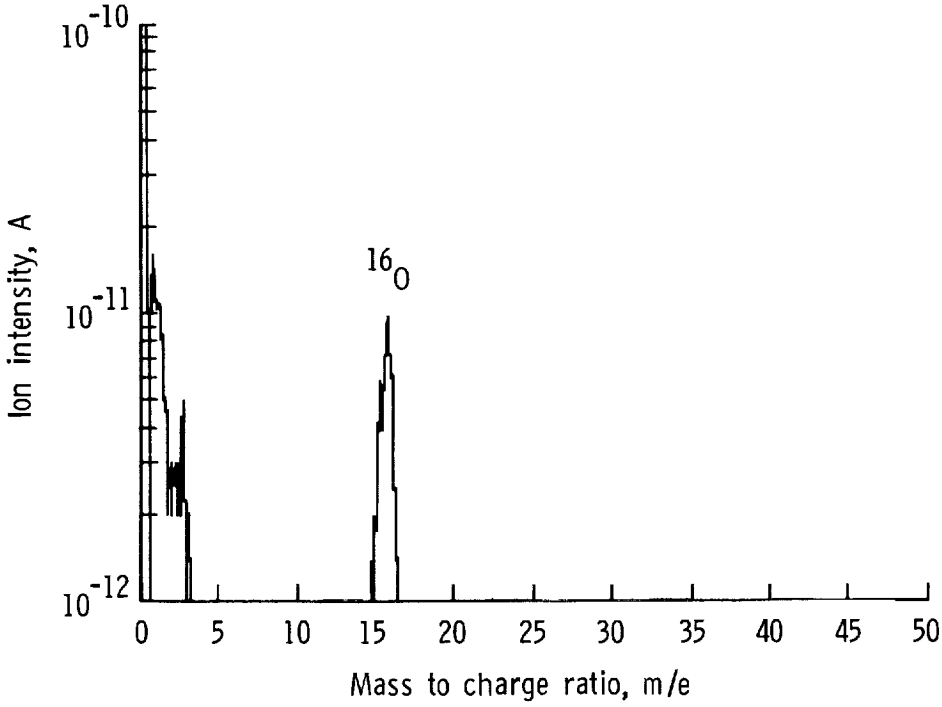

Figure 8. Mass survey of ESD species at $T_{Ag} = 300°C$ (AP mode).

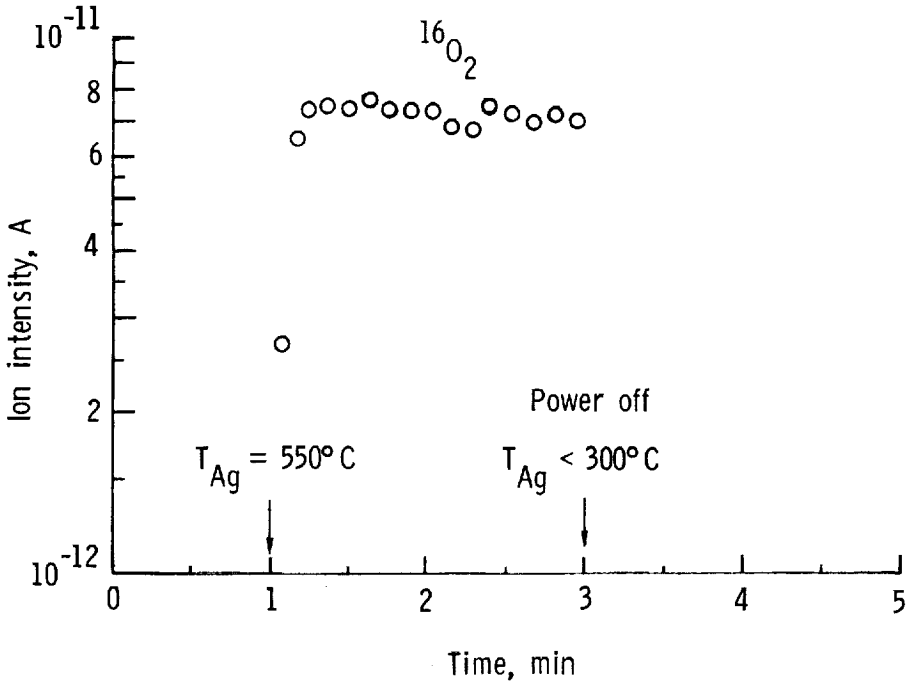

Figure 9. Thermal desorption of O_2 detected in AP mode.

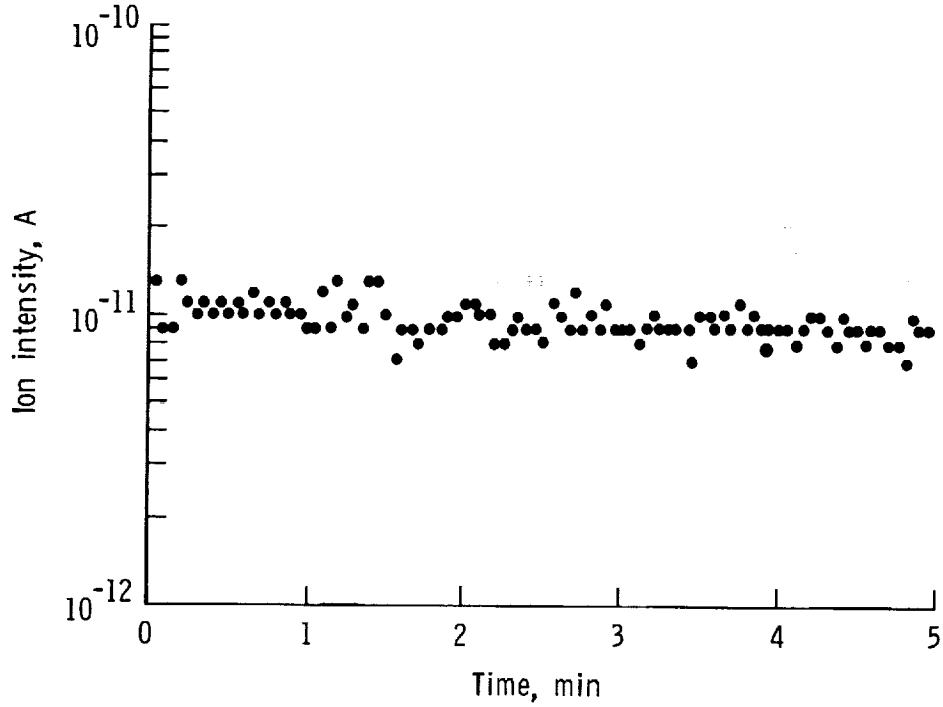

Figure 10. Decay of ESD ^{16}O signal because of reduction in bulk ^{16}O concentration (AP mode). $T_{Ag} = 300°C$.

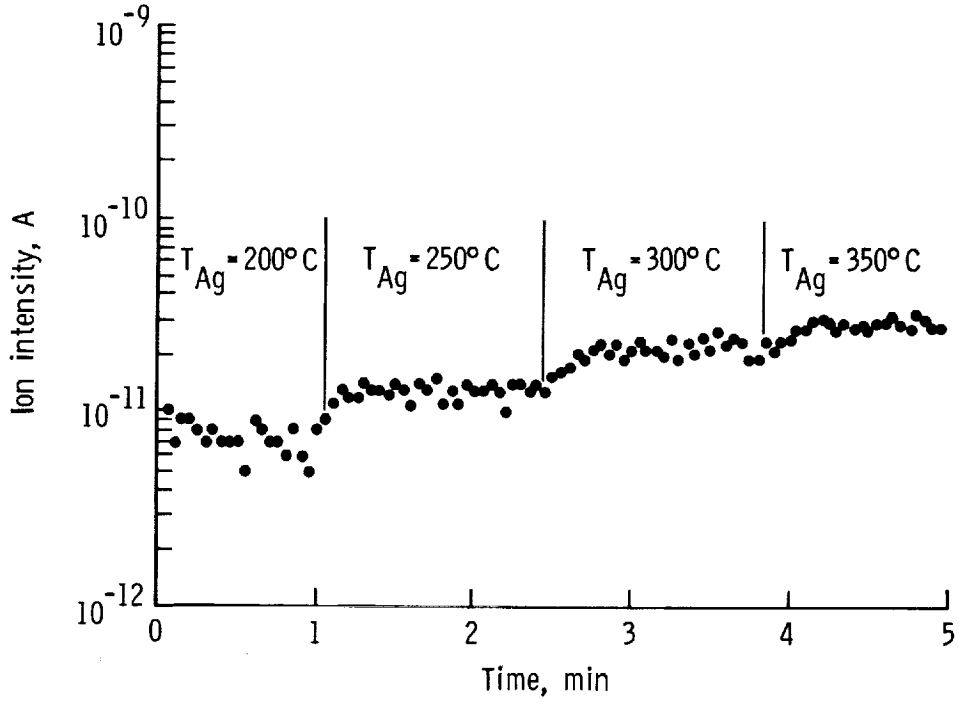

Figure 11. Variation in ESD ^{16}O signal as a function of Ag temperature (AP mode).

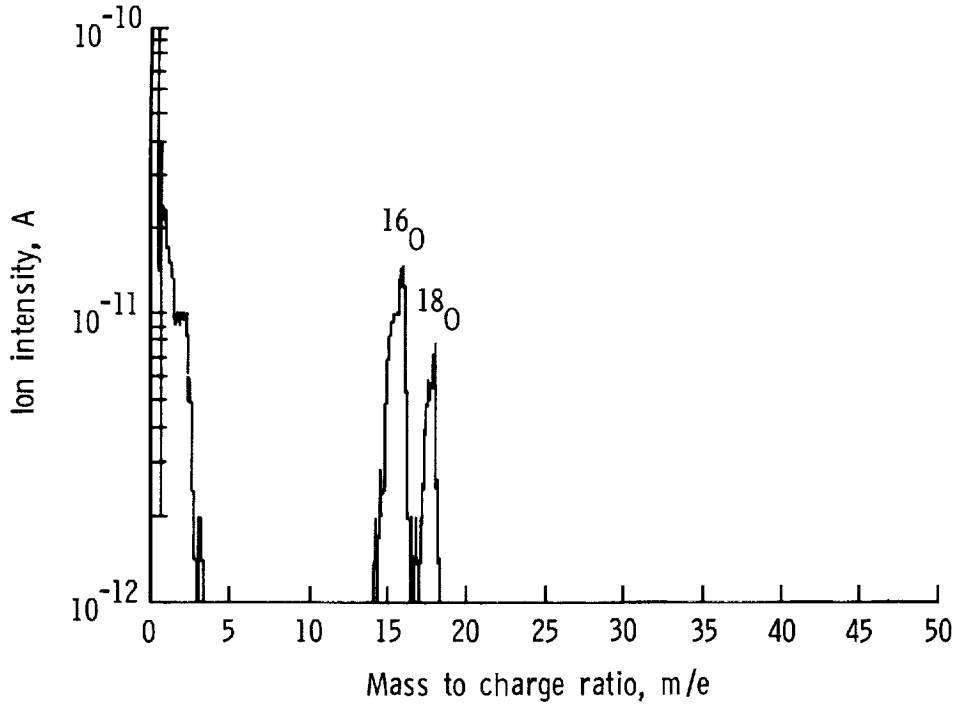

Figure 12. Mass survey spectrum of ESD species at $T_{Ag} = 200°C$ (AP mode).

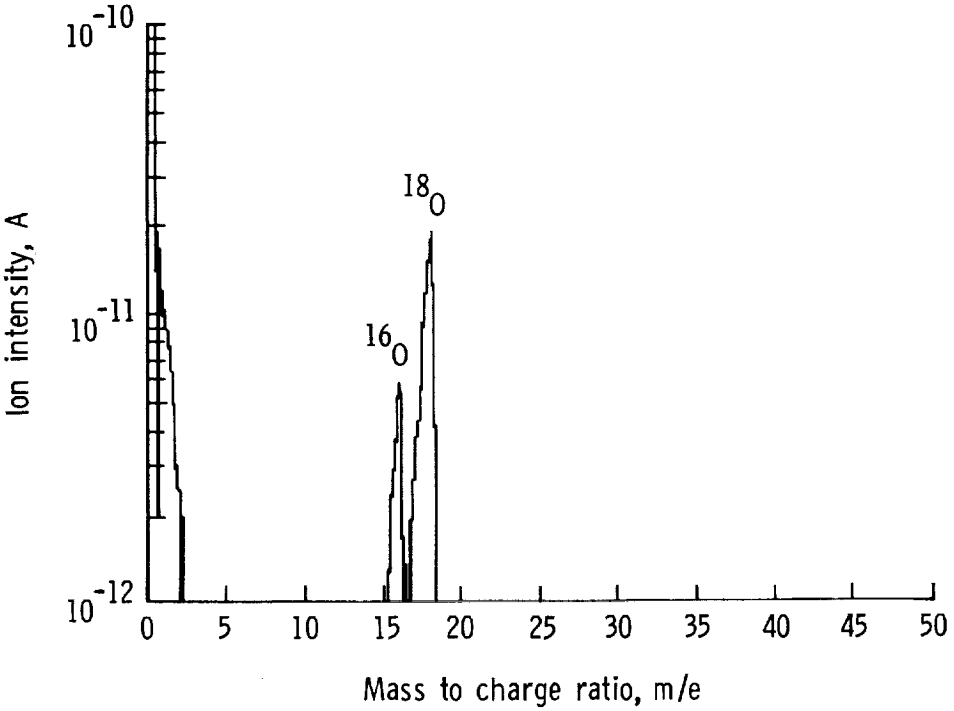

Figure 13. Mass survey spectrum of ESD species at $T_{Ag} = 450°C$ (AP mode).

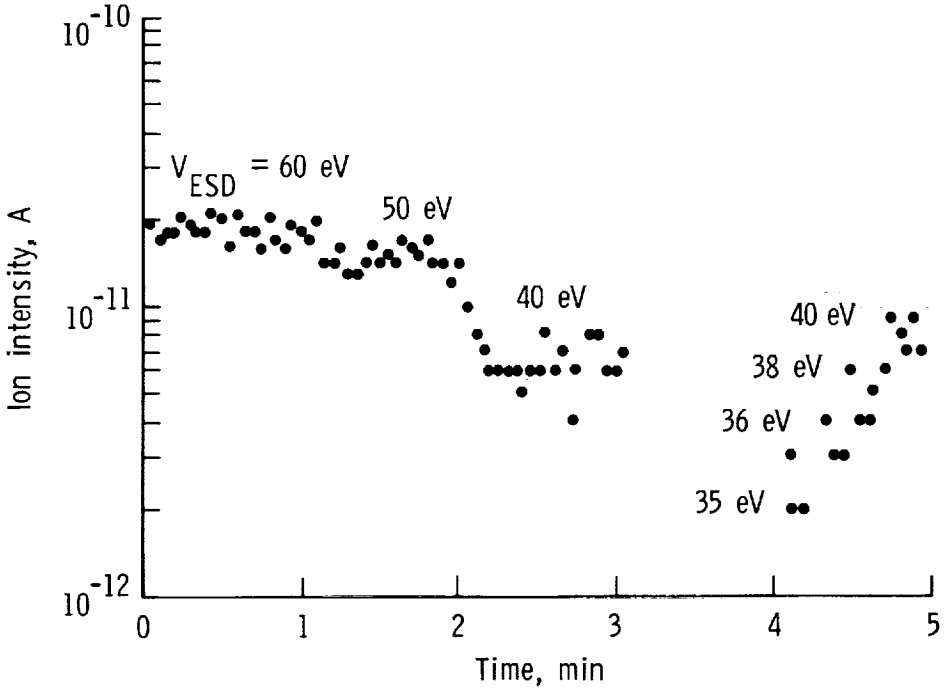

Figure 14. Variation in ^{18}O ESD signal as a function of electron impact voltage for $T_{Ag} = 450°C$ (AP mode).

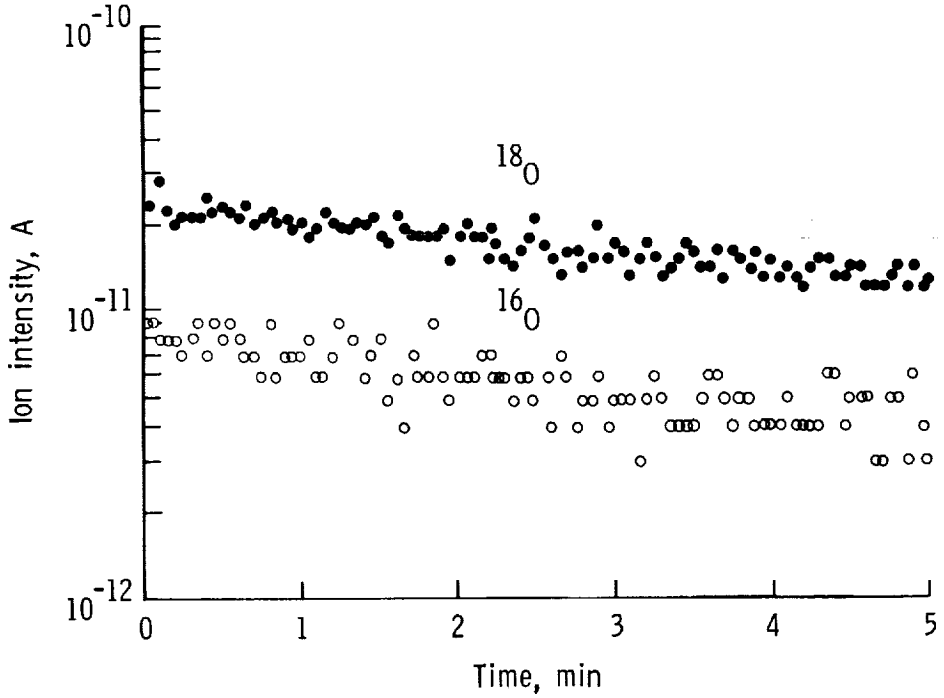

Figure 15. Decay of ^{18}O and ^{16}O ESD signals because of reduction in surface oxygen concentration as a function of time (AP mode). $T_{Ag} \approx 100°C$.

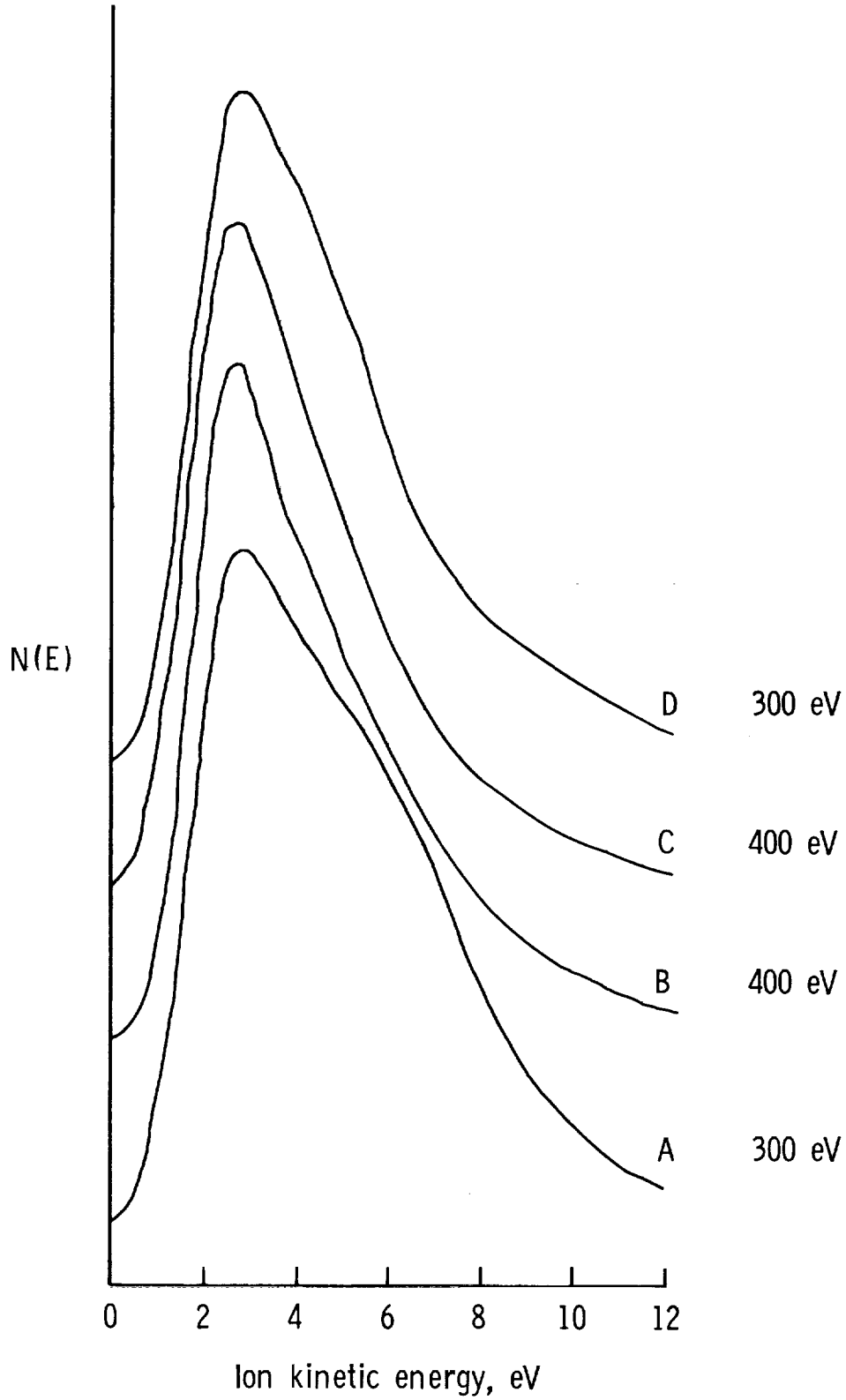

Figure 16. Electron-stimulated desorption ion energy distribution spectra with varying primary beam energy.

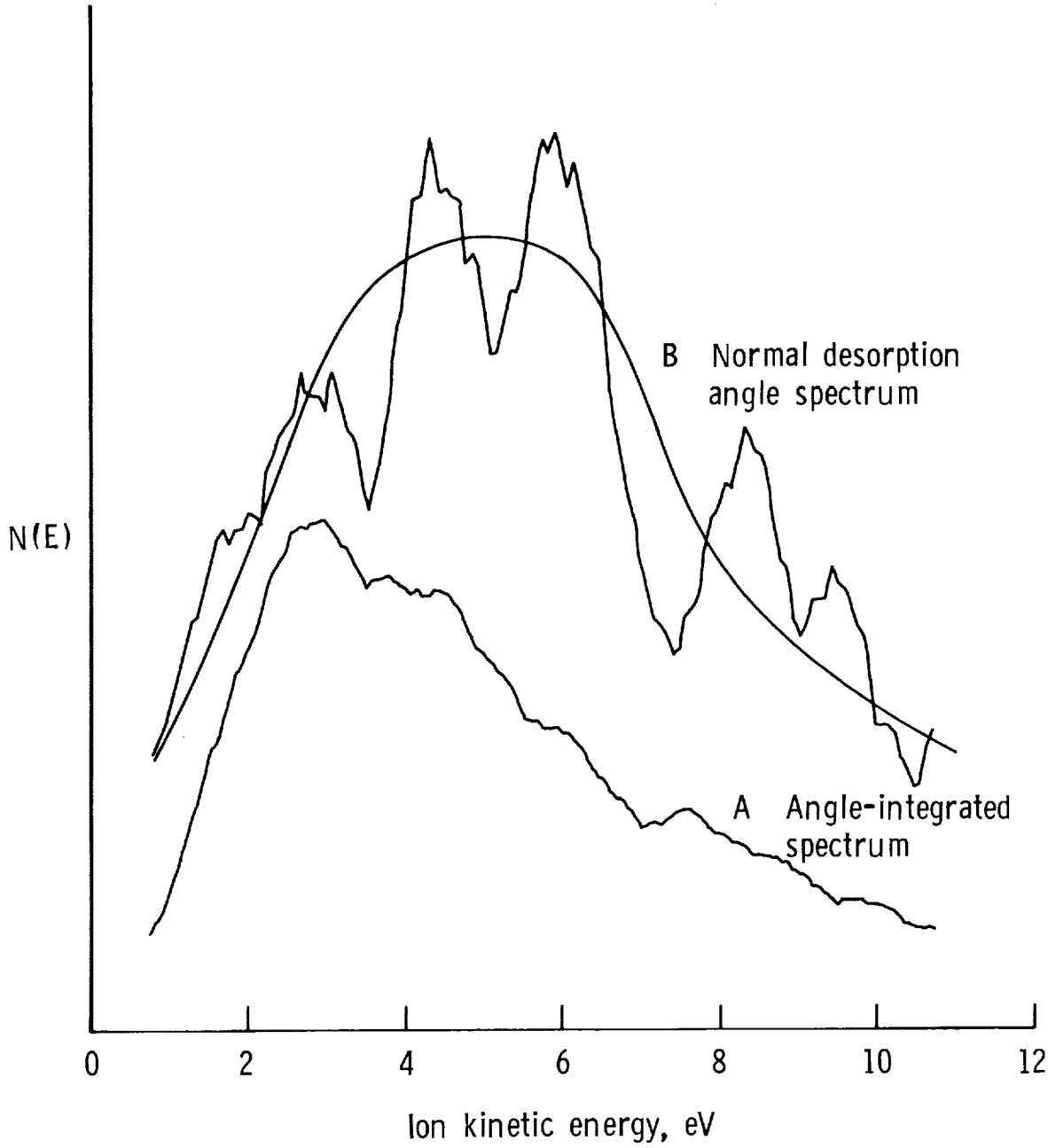

Figure 17. Angle-resolved ESD ion energy distribution spectra.

Standard Bibliographic Page

1. Report No.	2. Government Accession No.	3. Recipient's Catalog No.
NASA TP-2668		

4. Title and Subtitle	5. Report Date
Electron Stimulated Desorption of Atomic Oxygen From Silver	April 1987
	6. Performing Organization Code: 307-51-06-05
7. Author(s): R. A. Outlaw, W. K. Peregoy, Gar B. Hoflund, and Gregory R. Corallo	8. Performing Organization Report No.: L-16225
9. Performing Organization Name and Address: NASA Langley Research Center, Hampton, VA 23665-5225	10. Work Unit No.
	11. Contract or Grant No.
12. Sponsoring Agency Name and Address: National Aeronautics and Space Administration, Washington, DC 20546-0001	13. Type of Report and Period Covered: Technical Paper
	14. Sponsoring Agency Code

15. Supplementary Notes

R. A. Outlaw and W. K. Peregoy: Langley Research Center, Hampton, Virginia.
Gar B. Hoflund and Gregory R. Corallo: University of Florida, Gainesville, Florida.

16. Abstract

The electron stimulated desorption (ESD) of neutral oxygen atoms from polycrystalline silver and of oxygen ions from Ag(110) has been studied. Polycrystalline Ag charged with $^{16}O_2$ and $^{18}O_2$ and bombarded by low-energy electrons ($\approx$100 eV) under ultrahigh vacuum (UHV) conditions emitted O atom flux levels of 1×10^{12} cm^{-2}-s^{-1} at a Ag temperature of 300°C. The flux was detected with a quadrupole mass spectrometer operating in the appearance potential mode. The neutral cross section at about 100°C was determined to be 7×10^{-19} cm^2. Ancillary experiments conducted in a UHV chamber equipped with a cylindrical mirror analyzer and rigged for ion energy distribution and ion angular distribution were used to study O ions desorbed from Ag(110). Two primary O^+ energies of 2.4 and 5.4 eV were detected from the Ag(110) after having been dosed with 2500 L of $^{16}O_2$. It also appears that in both experiments there was strong evidence for directionality of the emitted flux. The results of this study serve as a proof of concept for the development of a laboratory atomic oxygen beam generator that simulates the gas flux environment experienced by orbiting vehicles.

17. Key Words (Suggested by Authors(s))	18. Distribution Statement
Atomic oxygen Electron stimulated desorption Neutral cross section Silver	Unclassified—Unlimited Subject Category 25

19. Security Classif.(of this report)	20. Security Classif.(of this page)	21. No. of Pages	22. Price
Unclassified	Unclassified	23	A02

For sale by the National Technical Information Service, Springfield, Virginia 22161

NASA-Langley, 1987